Measurement of high-temperature strains in superalloy and carbon/carbon composites using chemical composition gratings

Weihua Xie[1], Songhe Meng[1*], Hua Jin[1*], Chong Du[2], Shiyu Huo[1], Libin Wang[1], Tao Peng[1], Fabrizio Scarpa[3] and Chenghai Xu[1]

[1] Centre for Composite Materials and Structures, Harbin Institute of Technology, Harbin 150080, China

[2] Shanghai Advanced Research Institute, Chinese Academy of Sciences, Shanghai, China

[3] Advanced Composites Centre for Innovation and Science (ACCIS), University of Bristol, BS8 1TR Bristol, UK

Abstract: This paper describes an experimental and signal processing technique to perform high temperature tests on superalloy (INCONEL) and carbon/carbon structures using silica-based chemical composition gratings (CCGs). The results obtained from applying this technique at 940 °C in superalloys and 950 °C for carbon/carbon (C/C) composites are benchmarked against data obtained from four different methods. The results show that the wavelength responses of the CCGs bonded on the superalloy and on the C/C plate increase non-linearly with increasing temperatures. The temperature-dependent strain transfer coefficients recorded during the superalloy tests show quite stable results below 600 ^{o}C and tend to slightly decrase thereafter. The values of the strain transfer coefficients below 1000 °C are significantly affected by the thermal expansion coefficient of the substrate material and the interface. We demonstrate that the strain transfer coefficient calculation method used in this paper is not suitable for low and/or negative expansion material. The results of the relative errors show that the CCGs-F method based on the quadratic dependence of the wavelength shift versus the temperature appears to be the best to estimate the mechanical strains within the interval of temperatures considered and the measurement accuracy. The relative errors measured between 200 °C and 1000 °C are less than 5%.

Keywords: Fibre optics sensors; Strain and temperature; Chemical composition gratings; High-temperature application; Carbon-carbon; Superalloy;

1. Introduction

During high-speed or hypersonic flight the service temperature of thermal protection systems (TPS) and external airframe is generally higher than 1000 °C [1]. These significant hot environments make measuring the mechanical response of the structure a very difficult task, and provide substantial challenges in the design of hypersonic, re-usable launch vehicles and general spacecraft frames. In recent years high temperature Fibre Bragg Gratings (FBGs) sensors have shown promise for their potential use in extreme high-temperature environments. However,different types of materials possess different thermomechanical characteristics, and high temperature measurement technologies would need therefore to be developed based on the specific properties of the different materials under evaluation.

FBGs sensors exhibit a unique potential for aerospace applications due to their intrinsic configurability [2], light weight, reduced size, their immunity to electromagnetic and radiofrequency, long-distance transmission capabilities and good heat resistance [3, 4]. Two

* Corresponding author: Dr. Hua Jin, Email: jinhua2007@hit.edu.cn; Prof. Songhe Meng, Email: mengsh@hit.edu.cn

issues must be however resolved to facilitate and enlarge their field of applications. The first one is about how to produce a high temperature resistance sensor itself, while the second is about to how to fabricate the sensor on the real airframe designs. In previous studies, Fokine [5-10], Zhang [11, 12], Canning [13-16], Barrera [17-19], Guan [20-22], and other researchers [23-27] have developed significant activities focused around the fabrication of high temperature stable FBGs on different categories of host materials and topologies (i.e., type I, type II, and long-period gratings). Other topologies of FBGs previously described in open literature include photonic crystal fibres, sapphire gratings, and Chemical Composition Gratings (CCGs), which are commonly called Regenerated FBGs (RFBGs). RFBGs are typically produced in hydrogen-loaded optical fibres by applying an annealing treatment at temperatures between 800 °C and 1000 °C [28]. During the annealing process, the original grating is completely erased, and a new grating refractive index modulation that can withstand temperatures up to 1295 °C is created [13]. The main advantages of RFBGs compared with other optical sensing techniques are their ultrahigh temperature stability, good grating qualities, the possibility of measuring reflected light, and multiplexing capabilities. RFBGs sensor have now a higher technology readiness level degree after two decades of active research and development in this field. Recently, a significant body of research work has been devoted to the practical application of RFBGs. Méndez et al. [29, 30] , Selfridge et al. [31], Mamidi et al. [32], and Sai Prasad and co-workers [33] have bonded RFBGs onto metal substrates to measure the thermomechanical performance up temperatures of 900 °C. Reddy et al. [34], Barrera et al. [35, 36] and Azhari et al. [37] have attempted to encapsulate RFBGs within a metal or ceramic tube for usages up to 1100 °C. The packaging and installation of the sensors without damage on practical structures becomes however an import problem to the application of this technology, because silica-based RFBGs are very brittle and fragile after the annealing process [38].

In a previous work [39] we have described a simple method to apply CCGs sensors on ultra-high temperature ceramics materials (UHTCs) to measure strains up to 1000 °C. This method guarantees that the RFBGs are sensitive not only to the temperature, but also to the levels of strain occurring in the structure with respect to the optical fibre sensors encapsulated in the tube. Apart from UHTCs, carbon/carbon (C/C) and superalloys are widely used in the thermal protection systems of aerospace structures subjected to significant heat due to their high strength, thoughness at those elevated temperatures, their lightweight features and general and environmental durability [1]. In this paper, we present a thermo-mechanical measurement method suitable for applications on C/Cs and superalloys based on CCGs that can be applied to monitor airframe structures (see figure 1). The thermo-mechanical characteristics of the CCGs and the strain transfer coefficients are measured and analysed based on tests carried out on specific material specimens. The sensor bonding and measuring technique proposed in this paper combines simultaneous temperature and strain measurement in the structure, and allows to monitor the mechanical and thermal behaviour of superalloys and C/Cs material up to 940 °C and 950 °C, respectively. We also carry out a benchmark experiment to verify the methodology with two different instruments tocompare the accuracy of the thermal strain provided from the proposed CCGs.

2. Experimental details

The CCGs used in this study were fabricated with Ge-doped silica fibres at the Institute of Photonics Technology (Jinan University, China). The plate specimens can be heated rapidly along the thickness direction by a vertically mounted laser heater, which is a high-power fibre-coupled laser (DILAS Diodenlaser GmbH, Germany. Laser class: Compact-980.10-1500C, Output power: 1500 W, Wavelength: 980 nm±10 nm@25 °C). The diameter of the heating spot is 20mm, and the distance from the heating lens to the specimen is 200 mm. To simulate a realistic heating condition existing of the outer surfaces of airframes or spaceframes [40, 41], the specimen is heated vertically from the bottom. During the test, the laser heating lens is moved vertically and horizontally by adjusting a screw gear at the bottom of the laser heater. The temperature response of the specimen is recorded from a thermocouple

by using a multi-channel temperature signal acquisition instrument (LR8402-21, HIOKI, Japan). The overall temperature increase rate of the specimen is controlled with the adjustment of the laser heater output power, combined with the temperature response data.

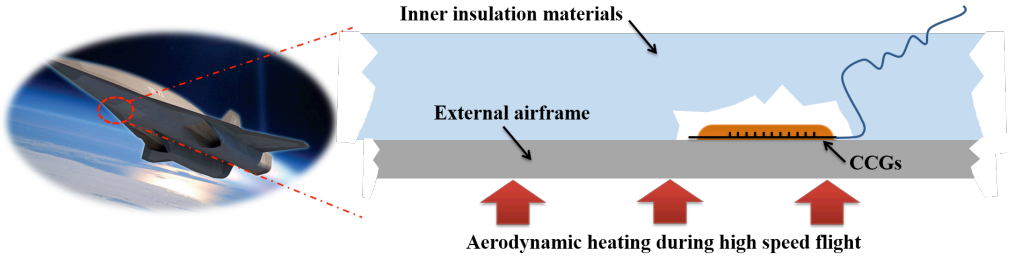

Figure 1. Schematic diagram of CCGs sensor installation in aerospace vehicle

The reflected wavelengths are acquired from an optical fibre grating demodulator (si425 Optical Sensing Interrogator, Micron Optics, Inc., USA). The wavelength shift of the CCGs is subjected to the combined effect of temperature and strain, and contains the effects of both the temperature changes on the CCGs itself and the strain provided by the thermal expansion of the structure caused by the temperature acting on the CCGs. Temperature compensation is adopted to decouple the CCGs signals [42] by installing a thermocouple at the same measurement location to record the temperature response of the grating. The thermocouple signal is used in experiments to eliminate the CCGs response wavelength caused by the temperature variation. When the wavelength shift caused by the temperature variations is removed from the overall signal the remaining part of the wavelength can be related to the strain measurements only.

In consideration of the surface properties and the mechanical performance of C/Cs and superalloys we use a high purity graphite adhesive (Resbond^{TM} 931C, COTRONICS CORP., USA) to connect the CCGs to the specimens. When the specimen is heated, the strain of the substrate material caused by the heat or deformation is transmitted to the grating in the form of a surface shear stress through the adhesive layer. Because of the contribution of the adhesive layer absorption to deformation, there is a difference between the grating and the actual sensed strains. This difference can be represented by a strain transfer coefficient β between the measured and the true strain. This coefficient directly depends upon the material of the structure, the physical characteristics of the adhesive and the geometry/size of the colloid used. It is possible to identify the values of the strain transfer coefficient from the experimental test data using the following equation [39].

$$\beta(T) = \frac{K_{T1} - (\alpha + \xi)}{K_\varepsilon(\alpha_s(T) - \alpha)} \tag{1}$$

Where K_ε=1-P_e is the strain sensitivity coefficient, and P_e=0.22 is the effective elastic-optic coefficient of fused silica [43]. The terms α_s and α denote the thermal expansion coefficient of the substrate material and the CCGs respectively. The value ξ is the thermo-optical coefficient of the CCGs. The term K_{T1} represents the coefficient of the first-order term if the relative variation of the measured total wavelength response $\Delta\lambda_B/\lambda_B$ is represented as a quadratic equation of temperature variations:

$$\frac{\Delta\lambda_B}{\lambda_B} = \frac{\Delta\lambda_T + \Delta\lambda_\varepsilon}{\lambda_B} = K_{T1}\Delta T + K_{T2}\Delta T^2 + C \tag{2}$$

In (2) K_{T2} represents the coefficient of the second-order term, and C is a universal constant. The parameter K_{T1} contains the effects of both the temperature changes on the CCGs itself and the strain provided by the thermal expansion of the structure caused by the temperature acting on the CCGs. Its value can be derived from post-processing experimental data. The wavelength shift $\Delta\lambda_T$ is caused by the temperature variations. The wavelength shift of the CCGs due to the strain corresponds to $\Delta\lambda_\varepsilon$, and it is affected by the strain and wavelength of CCGs, as well as the elastic-optic effect [44]. The theoretical relation of the strain sensitivity coefficient with the center wavelength and the strain variation is [39, 45, 46]:

$$\frac{\Delta\lambda_\varepsilon}{\lambda_B} = \Delta\varepsilon_s \beta K_\varepsilon \tag{3}$$

Where the center wavelength λ_B is the Bragg wavelength, $\Delta\varepsilon_s$ is the global strain of the structure, and it includes the thermal and structural strains.

3. Temperature and strain response characteristics from the tests

3.1. Superalloy

Two high temperature experimental tests are performed using two different CCGs with center wavelengths of 1551.275 nm (test #1) and 1550.450 nm (test #2). The installation of the superalloy and the CCGs is shown in figure 2(a). The superalloy samples (40 mm×45 mm×3 mm) consist in INCONEL® (nickel-chromium-iron) alloy 600. Two K-type thermocouples are installed at the end the adhesive layer. In order to facilitate the installation and operation of the sensor, the specimen is embedded in the insulating body, and therefore the surface of the specimen and the thermal isolation sit on the same work plane. In addition, the insulation package can provide support and insulation for the specimen. It is possible to note the circular area below which the laser heating occurs (figure 2(b)).

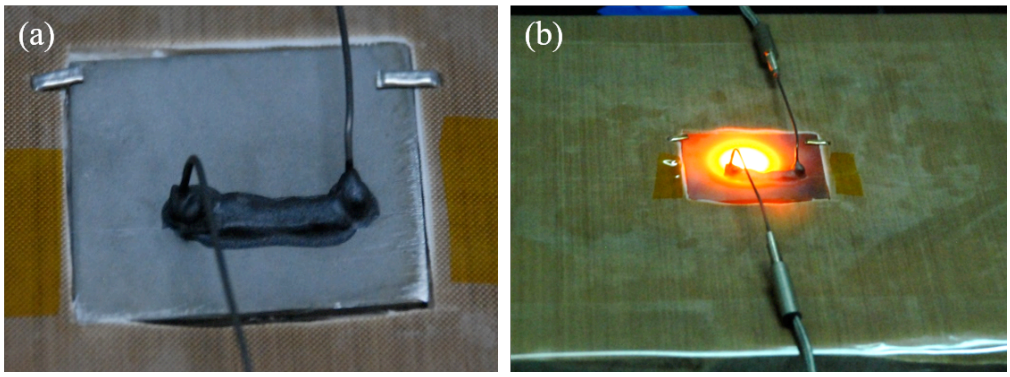

Figure 2. Images of the UHTCs specimen (a) before experiment and (b) during high temperature test

The highest temperature recorded during the tests is 940 °C and 923 °C for test #1 and test #2 respectively. The curves of the measured response signals of the CCGs versus the temperature are shown in figure 3. It is possible to observe that the response of the wavelength presents a nonlinear increase for rising temperatures. The nonlinearity is induced by the highly temperature-dependent thermo-optical coefficient and the thermal expansion coefficient of the silica fibre [47]. The response is also affected by the change of the periodicity of the Bragg grating of the fibre and the variation of the elastic-optic coefficient [48], hence the response exhibits a non-linearity. The wavelength maintains a steady upward trend except for some small sinusoidal fluctuations around 500 °C. These variations are similar to the wavelength shift shown in the curve in figure 4 of reference [39].

Here the relative variation of the wavelength is considered as the ratio between the wavelength increment and the center wavelength λ_B. A temperature compensation method is used to estimate the wavelength shift caused by the temperature variations. The relative variation of the wavelength caused by the strain can be obtained by using the total variation of the wavelength minus the variation of wavelength caused by temperature, i.e. $\Delta\lambda_\varepsilon/\lambda_B = \Delta\lambda/\lambda_B - \Delta\lambda_T/\lambda_B$. The value of $\Delta\lambda_T/\lambda_B$ can be obtained according to the relationship between the wavelength response and the temperature as shown in reference [39]. The temperature used during the compensation is recorded by a thermocouple. Figure 4 shows the results of the relative variation of the wavelength versus the temperature and the thermal strain of the specimen. Figure 4(a) also also shows the quadratic curve fitting of the experimental data, and table 1 lists the curve fitting parameters with a 95% confidence interval. Similar quadratic thermal responses were recorded in other works present in open literature [39, 46, 49, 50]. The average value of the parameter K_{T1} from table 1 can be used to calculate the average strain transfer coefficient β (table 2) from equation (1). After the strain transfer coefficient β is obtained, the global strain of the structure can be calculated by using equation (3), based on the reponse signal from the CCGs. The temperature dependence of the coefficient of thermal expansion (CTE) for the INCONEL® alloy 600 [51, 52] is taken into account to calculate the strain transfer coefficients, and the results are shown in table 2. The coefficients range from 0.574 to 0.714, and decrease gradually with increasing temperatures. When one compares the calculated strain transfer coefficient with the test data reported in reference [39] (see figure 9) it is possible to notice that the strain transfer coefficient will decrease for increasing temperatures. The coefficient however presents a decreasing trend trend from room temperature to 940 °C. The deviation of the test data under different conditions is mainly caused by the difference in the CCGs center wavelengths and the experimental methods used.

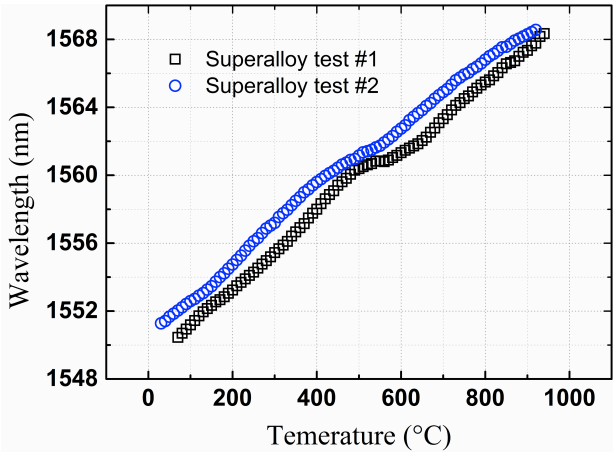

Figure 3. Wavelength variation of the CCGs sensors installed on the superalloy specimens.

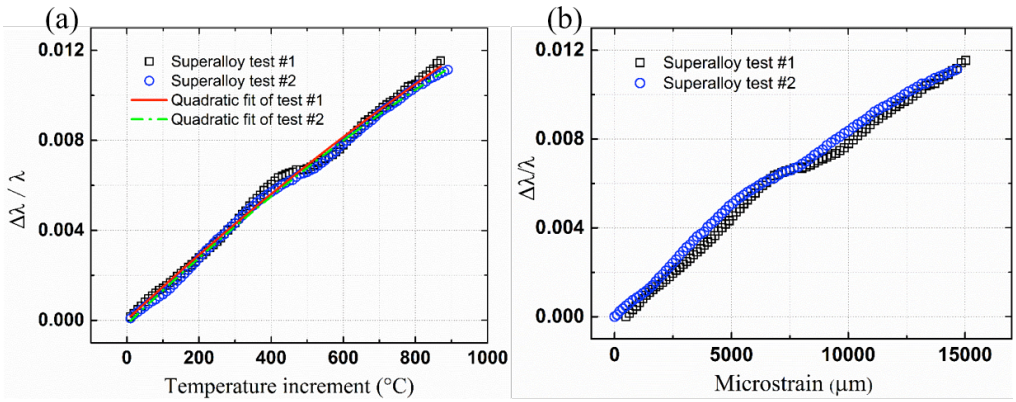

Figure 4. Relative variation of the wavelength for the INCONEL cases. (a) With increment of temperature. (b) With the thermal strain.

Table 1. Fitting parameters from the superalloy experimental data

Parameter	Superalloy test #1 (R^2=0.996)		Superalloy test #2 (R^2=0.998)	
	Value	Standard deviation	Value	Standard deviation
K_{T1}	1.48475E-5	7.01432E-5	1.53927E-5	2.42687E-7
K_{T2}	-2.19055E-9	3.67898E-7	-2.95097E-9	2.61274E-10
C	2.79605E-5	2.07932E-5	-1.7809E-4	4.73214E-5

Table 2. Average strain transfer coefficient from the superalloy experiments

Temperature (°C)	100	200	300	400	500	600	700	800	900
β	0.728	0.676	0.673	0.669	0.714	0.632	0.588	0.595	0.574

3.2. Carbon/carbon composites

The second test case for the application of the measurement technique consists in a three-dimensional carbon/carbon composite with a four direction (4D) microstructure. The 4D C/C composite woven has axial carbon rods with ~70% volume fraction of fibres, and the architecture contains 0°/60°/120° in-plane bundles in the XY plane and Z-directional bundles (figure 5). This C/C composite was prepared using pressure impregnation and carbonization (PIC), followed by high pressure impregnation and carbonization (HPIC), and high temperature treatment (HTT) [53, 54]. The final density of the 4D C/C composite is close to 1.9 g/cm^3.

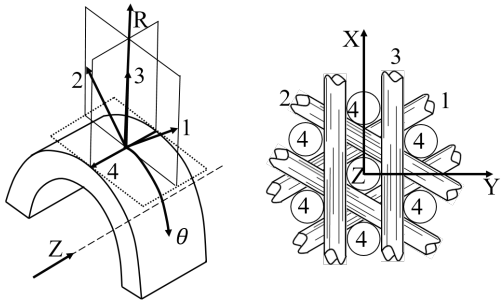

Figure 5. Braid configuration of 4D C/C composites.

As shown in figure 6, the CCGs (dimensions 40 mm×45 mm×5 mm) are bonded to the C/C sample along the Z-axis on the ZX plane with adhesive (Resbond 931C, COTRONICS CORP., USA). A test has been carried out with CCGs sensors with a center wavelength of

1550.811 nm. The average maximum peak temperature reached 950 °C, and the color of the sample changed from red to orange-yellow, as shown in figure 6(b). The response wavelength signals of the CCGs have been recorded when the sample was heated. Figure 7(a) shows the relation between the wavelength response and the temperatures. The wavelength maintains a steady nonlinear upward trend for increasing temperature except for small fluctuations around 500 °C. Figure 7(b) describes the relative variation of the wavelength response in the C/C specimen with the quadratic fitting of equation (1) and related parameters with 95% confidence interval shown in table 3.

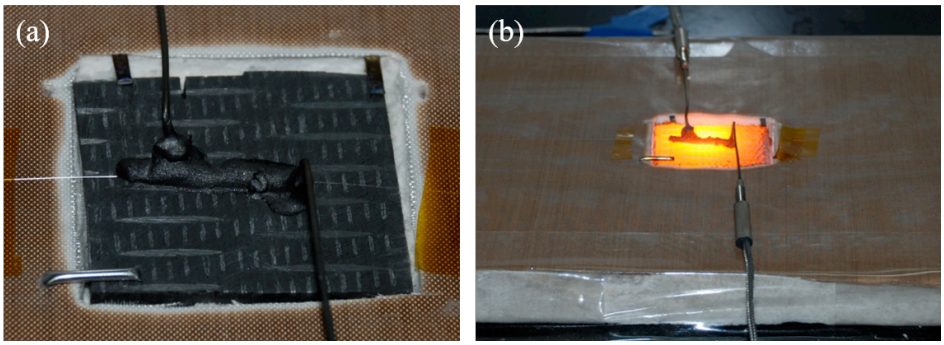

Figure 6. Images of the C/C specimen (a) before experiment and (b) during the high temperature test

It is important to note that we cannot follow the same process to compute the thermal strain variation of the specimen and the relative variation of the wavelength from the data in figure 4(b) because of the complexity of the coefficient of linear thermal expansion (CTE) of the 4D C/C composite. The value of K_{T1} in table 3 is quite different with the values from the superalloy tests in table 2 and the analogous values of ultra-high-temperature ceramics (UHTCs) in reference [39]. In this case the parameter K_{T1} contains the effects of both the temperature changes on the CCGs itself and the strain provided by the thermal expansion of the structure, so its value should be larger than the temperature sensitivity coefficient of the bare fibers, which is 7.780×10^{-6} as reported in reference [50]. For a silica based pristine fiber the parameter K_{T1} is theoretically equal to the sum of the thermal expansion coefficient α and the thermo-optic coefficient ξ, and it varies in a range between $7\times10^{-6}\,^{o}C^{-1}$~$11\times10^{-6}\,^{o}C^{-1}$[37, 55-57]. Since the value of K_{T1} in table 3 is even lower than the minimum theoretical value, it can be inferred that the thermal strain of the C/C composite has a negative impact on the response wavelength of the CCGs. A major feature of C/C materials is the negative thermal expansion characteristic from room temperature to 400 ºC [58, 59], and even at 800 ºC [60]. The CTE of the 4D composite varies from $-1.0\times10^{-6}\,^{o}C^{-1}$ to $3\times10^{-6}\,^{o}C^{-1}$ [53, 58-60] in the range from room temperature to 1000 ^{o}C, but the CTE of the adhesive (Resbond^{TM} 931C) is $7.38\times10^{-6}\,^{o}C^{-1}$ (value provided by COTRONICS CORP). Due to the low thermal expansion properties of the C/C structure, the thermal strain of the carbon composite is significantly lower than the one of the adhesive layer. It is possible to note that the C/C specimen will prevent the thermal expansion of the adhesive layer and the CCGs during the heating process, and even have a negative impact on the thermal strain of the adhesive layer and CCGs. In this case, the thermal strain of the specimen can not be calculated by the methods proposed in this work.

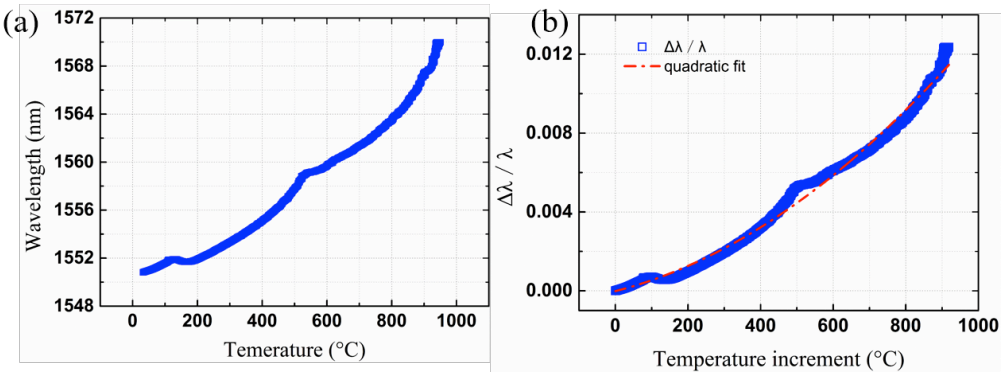

Figure 7. Wavelength variation of the CCGs sensors installed on the C/C sample. (a) Variation with temperature. (b) Relative variation with increasing temperature.

Table 3. Fitting parameters of C/C experiments data (R^2=0.991)

Parameter	Value	Standard deviation
K_{T1}	4.69269E-6	8.45042E-8
K_{T2}	8.48914E-9	8.26062E-11
C	-1.46321E-5	1.87659E-5

4. Verification tests

4.1. experimental design

To verify the data estimated by means of the CCGs and the validity of the measurement of the strain transfer coefficient, additional tests have been completed to record the thermal strain independently by using high-temperature strain gauges (HFH-12-250-ZHW, Maximum service temperature: 816 °C, USA) and 2D laser displacement sensor (LJ-G030, Keyence corporation, Japan) to verify the strain data. An infrared camera (VarioCAM® HiRes sl, JENOPTIK Infra Tec.) is also used to verify the temperature. Figure 8 shows the layout of the CCGs verification tests. The strain gauge and the CCGs are bonded symmetrically to obtain a simultaneous measurement of the response of the specimen. Another unbonded strain gauge is arranged in the same horizontal position, symmetrical to the longitudinal center line, to produce the temperature compensation signal. Two support narrow adhesive layer segments are made vertically to CCGs. The dash line AB in figure 8(a)is selected as the test region of the 2D laser displacement sensor. The red line near the white layer (figure 8(b)) indicates the 2D laser measure region. The strain can be derived by the variation of the length of line AB. Two K-type thermocouples are glued to measure the temperature on the symmetrical positions of the CCGs.

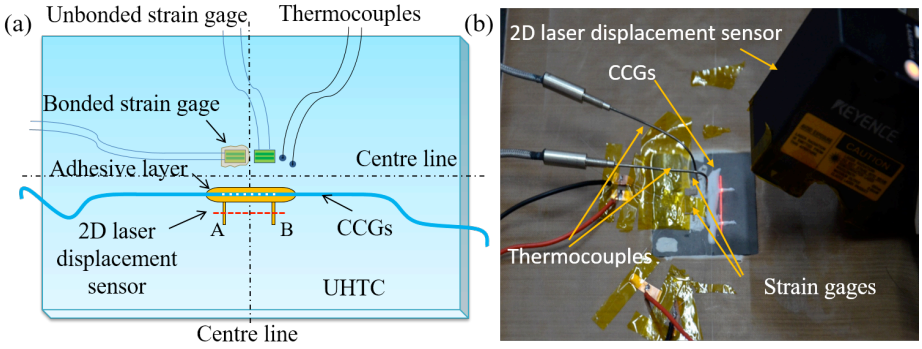

Figure 8. Experimental rig for the CCGs verification test. (a) Layout of the measurement. (b) Image of the sensors installed.

Two tests have been carried out on UHTC specimens (50 mm×50 mm×5 mm) to verify the measuring accuracy. In the first verification test the 2D laser displacement sensor did not work when the temperature exceeded 600 °C, because the red line of the laser was covered by the red light emitted by the specimen, which made the 2D laser displacement sensor non usable. It has to be noted however that the 2D laser displacement sensor can not be used efficiently in environments above 50 °C, so the strain data obtained by this method are not valid to be used as an evaluation criteria above that threshold temperature. In the second verification test the strain gauge is used as the only reference sensor, and two K-type thermocouples are placed on the adhesive layer directly. The strain gauge stopped working at 780 °C before reaching its maximum operating temperature of 816 °C. On the contrary, the CCGs with center wavelengths of 1550.316 nm have shown an excellent performance up to 1047 °C. The CCGs sensors show therefore a higher flexibility and broader range than the strain gauge in terms of temperature.

4.2. Results and discussions

Figure 9 shows the temperature distribution on the UHTC specimen when the external temperature exceeds 1000 °C. It is possible to to observe that the area corresponding to the temperature of the measuring region has the highest values (1000 °C~1100 °C - see figure 9(b)). This observation is consistent with the recorded results from the thermocouples. The temperature contour is not symmetrical because of the presence of the strain gages and the adhesive layer. The temperature distribution is however more uniform in other regions apart from the central area.The connecting wires of the strain gauges can also be observed in the image.

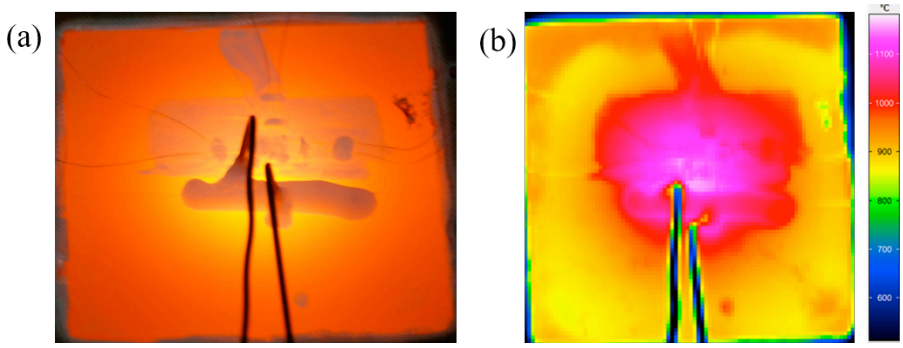

Figure 9. Temperature distribution on the UHTC specimen. (a) Photo. (b) Image from the infrared temperature camera.

Figure 10 shows the results from the quadratic curve fitting of the relative variation of the wavelength versus the temperature. From the previous observations of figure 4(a), 7(b) and 10 it is possible to note that the wavelength data tend to fluctuate at about 500 °C. One reason for this behavior is that when the steady-state temperature of the specimen and the adhesive reaches approximately 500 °C, the inner microstructure of the adhesive layer begins to change, as part of the adhesive has softened at this temperature level. This change in microstructure leads to a change of the interface state between the adhesive and the CCGs, as well as between the adhesive and the substrate material. The consequence of these changes in the interface behavior significantly affects the strain transfer of the specimen to the CCGs, and therefore the CCGs signals will fluctuate.

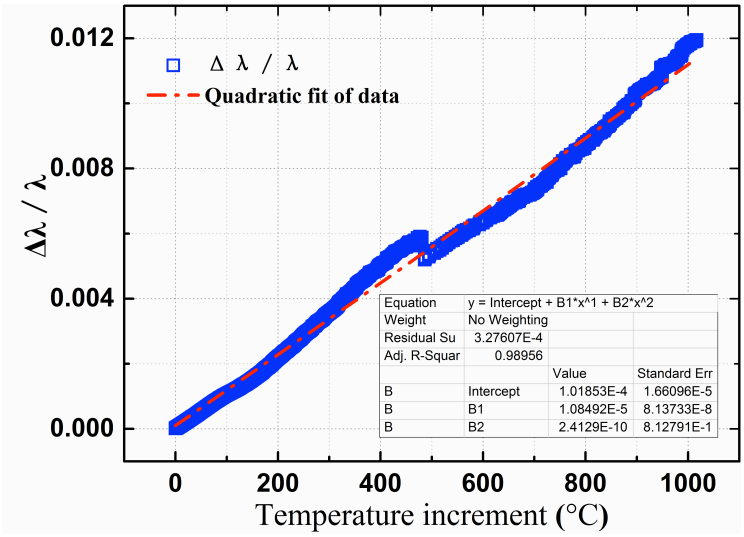

Figure 10. Relative variation of the CCGs wavelength with the temperature increment.

After the relative variation of the measured total wavelength response $\Delta\lambda_B/\lambda_B$ is obtained from the experimental wavelength data, it can be used to calculate the term $\Delta\lambda_\varepsilon/\lambda_B$ through the temperature compensation method. After the relative variation of the wavelength response caused by strain is obtained, the global strain $\Delta\varepsilon_s$ of the specimen can be calculated by using equation (3) and the strain transfer coefficient of reference [39]. During this process, the total wavelength response $\Delta\lambda_B/\lambda_B$ can be derived using two approaches. The first one consists in just using the original measured experimental data, and we will denote this approach as CCGs-O. The other is about using the quadratic fit curve data to eliminate the fluctuation test data, and the corresponding strain will be denoted in this case as CCGs-F. The strains derived from the different methods are presented in figure 11. It is possible to obseve that the CCGs-F curve compares quite well with the theoretical data. Although the CCGs-F curve does not show the same level of agreement it presents a similar trend with the relative variation of the wavelength. In these measurements it is still present the fluctuation around 500 °C largely induced by the mismatch between CCGs, adhesive layer and substrate material. The strains measured by the strain gauges and the 2D laser displacement sensor are also indicated in figure 11. It is possible to notice that the curve related to the strain gauges measurements fluctuates significantly, but its oscillating centerline is around the theoretical value before 600 °C. Although the 2D laser displacement sensor can not be used when the temperature exceeds 50 °C, the strain value measured by it seems to follow the theoretical value to some degree. It should be also noted that the values presented are affected by the noise reduction filter chosen in software MATLAB® Comparing all the above results , it is apparent that the CCGs-F systems appears to be the most suitable to describe the global strain of the specimen.

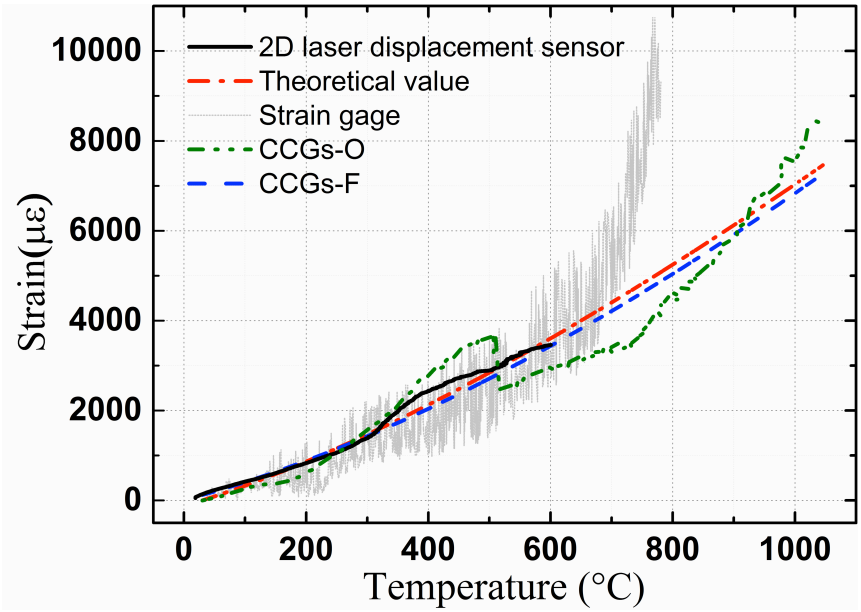

Figure 11. Strain curves of the different verify methods.

The relative strain errors measured by the four methods used in this work are presented in table (4). The relative error for each temperature was averaged within the range of ±5 °C. The relative errors of the CCGs-O and strain gauges methods are around 20~30%, and quite larger than the results provided by the other two methods. In the case of the high-temperature strain gauges, the sensors used for temperature and compensation are very hard to fix on the present position by non-bonding, especially in high temperatures environments. The relative error is therefore large and due to the uncertainty of the temperature compensation. In the case of the CCGs-O method the strain is mainly affected by the mismatch between the CCGs, adhesive layer and substrate during heating, which makes the wavelength data fluctuate around 500 °C. In fact, the main reason of the CCGs-F method generating a large-scale error is that the relative variation of the wavelength caused by the strain during the test is very small, less than 1/3 of the total amount of variation after 200 °C. In this case, any small changes during the tests can cause dramatic variations in the strain results. Although the relative errors provided by the 2D laser are below 15% when the temperature is above 100 °C these data cannot be used as valid because they are measured beyond the instrument operating temperature, the measuring red laser light being affected by the high-temperature specimen emissive red light. The relative errors given by the CCGs-F method are all within 5% except at 100 °C. At low temperatures (below 200 °C) the total increment of the wavelength is small and the relative variation of the wavelength caused by strain is even smaller, causing large relative errors due to the accuracy of the demodulator. Results obtained by the CCGs-F method can eliminate the influence of some uncertainty factor, and provide in general the better fits to the actual structural strain existing within the structure within the range of 200 °C ~ 1000 °C.

Table 4. Relative errors provided by the different methods compared with the theoretical thermal expansion strain

Methods†	100 °C	200 °C	300 °C	400 °C	500 °C	600 °C	700 °C	800 °C	900 °C	1000 °C
CCGs-O	19.78%	30.15%	7.75%	31.02%	27.39%	18.36%	23.44%	14.57%	3.86%	7.94%
CCGs-F	23.38%	2.06%	2.61%	4.18%	4.65%	4.63%	4.35%	3.91%	3.38%	2.81%
Strain gauges	15.97%	46.38%	23.92%	32.22%	26.06%	15.04%	18.23%	/	/	/
2D Laser	26.97%	4.00%	5.19%	14.17%	1.2%	3.80%	/	/	/	/

†: CCGs-O - strain value derived from the original wavelength data; CCGs-F - strain derived from the quadratic fit curve of the original wavelength data.

5. Conclusions

In this work we have presented a detailed study on high temperature application and measurement benchmark of chemical composition gratings. High temperature tests show that high purity graphite adhesive can be used to bond the CCGs to both superalloy and carbon/carbon composite materials up to a temperature of 950 °C. A signal decoupling technique based on temperature compensation and a specific strain transfer coefficient calculation methodology based on the effect of the adhesive absorption have been used to analyse the structural thermal strain response from room temperature to 950 °C. The results show that the wavelength and strain responses signal increase non-linearly with increasing temperatures. The strain transfer coefficient is significantly affected by the CTEs of the substrate material and the interface, and the corresponding value from the superalloy test varies between 0.574 and 0.728. This method cannot be however used on the C/C composite due to its lower and negative thermal expansion coefficient. Four different methods have been evaluated to verify the accuracy of the CCGs measurements. The results from the relative errors show that the CCGs-F technque is the most suitable to estimate the structural strains in terms of operating temperature range and measurement accuracy, and the relative errors between 200 °C and 1000 °C are lower than 5%. Although further investigations are needed to discover the mechanism of fluctuations around 500 °C, the work described in this paper provides a simple and efficient method to apply silica-based optical fibre sensors on practical aerospace structures to measure strains at high temperatures up to 950 °C.

Acknowledgments

This research was supported by the Project of National Natural Science Foundation of China (11272107, 11472092 and 11502058), National Basic Research Program of China (2015CB655200). The authors thank Institute of Photonics Technology (Jinan University, Guangzhou, China) for providing the CCGs sensors. The authors also thank Dr. Xinyang Sun and Dr. Zhichun Zhang for their assistance with the verification test.

References

1. Glass D.E. (2008) Ceramic matrix composite (CMC) thermal protection systems (TPS) and hot structures for hypersonic vehicles. Proc. 15th AIAA space planes and hypersonic systems and technologies conference, 1-36.
2. Panopoulou A., Roulias D., Loutas T. and Kostopoulos V. (2012) Health monitoring of aerospace structures using fibre Bragg gratings combined with advanced signal processing and pattern recognition techniques. *Strain* **48**: 267-277.
3. Culshaw B. (2000) Measuring strain using optical fibres. *Strain* **36**: 105-113.
4. Bennion I., Zhang L. and Everall L. (2000) In‐Fibre Grating Techniques for Strain Sensing. *Strain* **36**: 115-121.
5. Fokine M. (2002) Thermal stability of chemical composition gratings in fluorine–germanium-doped silica fibers. *Opt Lett* **27**: 1016-1018.
6. Fokine M. (2002) Photosensitivity, chemical composition gratings and optical fiber based components. PhD, Royal Institute of Technology.
7. Fokine M. (2002) Formation of thermally stable chemical composition gratings in optical fibers. *JOSA B* **19**: 1759-1765.
8. Pal S., Mandal J., Sun T., Grattan K., Fokine M., Carlsson F., Fonjallaz P.Y., Wade S. and Collins S. (2003) Characteristics of potential fibre Bragg grating sensor-based devices at elevated temperatures. *Measurement Science and Technology* **14**: 1131.
9. Fokine M. (2004) Thermal stability of oxygen-modulated chemical-composition gratings in standard telecommunication fiber. *Opt Lett* **29**: 1185-1187.

10. Holmberg P., Laurell F. and Fokine M. (2015) Influence of pre-annealing on the thermal regeneration of fiber Bragg gratings in standard optical fibers. *Opt Express* **23**: 27520-27535.
11. Zhang B. (2007) Optical high temperature sensor based on fiber bragg grating. PhD, Concordia University, Montreal, Canada.
12. Zhang B. and Kahrizi M. (2007) High-temperature resistance fiber Bragg grating temperature sensor fabrication. *Sensors Journal, IEEE* **7**: 586-591.
13. Canning J., Stevenson M., Bandyopadhyay S. and Cook K. (2008) Extreme silica optical fibre gratings. *Sensors* **8**: 6448-6452.
14. Bandyopadhyay S., Canning J., Stevenson M. and Cook K. (2008) Ultrahigh-temperature regenerated gratings in boron-codoped germanosilicate optical fiber using 193 nm. *Opt Lett* **33**: 1917-1919.
15. Canning J., Stevenson M., Fenton J., Aslund M. and Bandyopadhyay S. (2009) Strong regenerated gratings. Proc. 20th International Conference on Optical Fibre Sensors, 750326-750326-750324.
16. Canning J., Cook K., Aslund M., Stevenson M., Biswas P. and Bandyopadhyay S. (2010) *Regenerated fibre Bragg gratings* INTECH Open Access Publisher.
17. Barrera D., Finazzi V., Coviello G., Bueno A., Sales S. and Pruneri V. (2010) Chemical composition gratings in Germanium doped and Boron-Germanium co-doped fibers. Proc. SPIE Photonics Europe, 772607-772607-772607.
18. David B., Vittoria F., Joel V., Antonio B., Salvador S. and Valerio P. (2010) On the use of optical fiber sensors (CCGs and PCFI) for harsh environments. Proc. Waves, 128-133.
19. Barrera D. (2010) Fiber-optic sensors for high-temperature applications. *SPIE Newsroom* **6**.
20. Li G. and Guan B.-o. (2010) Research on reflectivity of chemical composition grating sensors at high temperatures. Proc. Asia Communications and Photonics Conference and Exhibition, 79860U-79860U-79865.
21. Li G. and Guan B.o. (2011) Improvement on reflectivity of chemical composition gratings at high temperatures. *Microw Opt Technol Let* **53**: 963-966.
22. Li G., Liu M., Li Y. and Guan B.o. (2012) Fabrication and sensing characteristics of the chemical composition grating sensor at high temperatures. *Microw Opt Technol Let* **54**: 71-75.
23. Grobnic D., Smelser C.W., Mihailov S.J. and Walker R.B. (2006) Long-term thermal stability tests at 1000 C of silica fibre Bragg gratings made with ultrafast laser radiation. *Measurement Science and Technology* **17**: 1009.
24. Coviello G., Finazzi V., Villatoro J. and Pruneri V. (2009) Thermally stabilized PCF-based sensor for temperature measurements up to 1000 C. *Opt Express* **17**: 21551-21559.
25. Cheong Y., Chong W., Chong S., Lim K. and Ahmad H. (2014) Regenerated Type-IIa Fibre Bragg Grating from a Ge–B codoped fibre via thermal activation. *Optics & Laser Technology* **62**: 69-72.
26. Laffont G., Cotillard R. and Ferdinand P. (2013) Multiplexed regenerated fiber Bragg gratings for high-temperature measurement. *Measurement Science and Technology* **24**: 094010.
27. Lindner E., Canning J., Chojetzki C., Brückner S., Becker M., Rothhardt M. and Bartelt H. (2011) Thermal regenerated type IIa fiber Bragg gratings for ultra-high temperature operation. *Opt Commun* **284**: 183-185.
28. Bueno A., Kinet D., Mégret P. and Caucheteur C. (2013) Fast thermal regeneration of fiber Bragg gratings. *Opt Lett* **38**: 4178-4181.
29. Méndez A., Wnuk V.P., Fokine M., Claesson Å., Nilsson L.-E., Ferguson S. and Graver T. (2005) Packaging process of fiber Bragg grating strain sensors for use in high-temperature applications. Proc. Optics East 2005, 60040E-60040E-60047.
30. Wnuk V.P., Méndez A., Ferguson S. and Graver T. (2005) Process for mounting and packaging of fiber Bragg grating strain sensors for use in harsh environment applications. Proc. Smart Structures and Materials, 46-53.

31. Selfridge R.H., Schultz S.M., Lowder T.L., Wnuk V.P., Méndez A., Ferguson S. and Graver T. (2006) Packaging of surface relief fiber Bragg gratings for use as strain sensors at high temperature. Proc. Smart Structures and Materials, 616702-616702-616707.
32. Mamidi V.R., Kamineni S., Ravinuthala L.S.P., Thumu V. and Pachava V.R. (2014) Characterization of Encapsulating Materials for Fiber Bragg Grating-Based Temperature Sensors. *Fiber Integrated Opt* **33**: 325-335.
33. Reddy P.S., Sai Prasad R.L., Srimannarayana K., Sai Shankar M. and Sen Gupta D. (2010) A novel method for high temperature measurements using fiber Bragg grating sensor. *Opt Appl* **40**: 685-692.
34. Reddy P.S., Prasad R.L.N.S., Gupta D.S., Shankar M.S., Narayana K.S. and Kishore P. (2011) Encapsulated fiber Bragg grating sensor for high temperature measurements. *Opt Eng* **50**: 114401-114401-114406.
35. Barrera D., Finazzi V., Villatoro J., Sales S. and Pruneri V. (2011) Performance of a high-temperature sensor based on regenerated fiber Bragg gratings. Proc. 21st International Conference on Optical Fibre Sensors (OFS21), 775381-775381-775384.
36. Barrera D., Finazzi V., Villatoro J., Sales S. and Pruneri V. (2012) Packaged optical sensors based on regenerated fiber Bragg gratings for high temperature applications. *Sensors Journal, IEEE* **12**: 107-112.
37. Azhari A., Liang R. and Toyserkani E. (2014) A novel fibre Bragg grating sensor packaging design for ultra-high temperature sensing in harsh environments. *Measurement Science and Technology* **25**: 075104.
38. Mihailov S.J. (2012) Fiber Bragg grating sensors for harsh environments. *Sensors* **12**: 1898-1918.
39. Xie W., Meng S., Jin H., Du C., Wang L., Peng T., Scarpa F. and Huo S. (2016) Measurement of the high-temperature strain of UHTC materials using chemical composition gratings. *Measurement Science and Technology* **27**: 055101.
40. Latini V., Striano V., Coppola G. and Rendina I. (2007) Fiber optic sensors system for high-temperature monitoring of aerospace structures. Proc. Microtechnologies for the New Millennium, 65930S-65930S-65939.
41. Manor D., Lau K.Y. and Johnson D.B. (2005) Aerothermodynamic environments and thermal protection for a wave-rider second stage. *J Spacecraft Rockets* **42**: 208-212.
42. Ge Y., Elshafie M.Z., Dirar S. and Middleton C.R. (2014) The response of embedded strain sensors in concrete beams subjected to thermal loading. *Constr Build Mater* **70**: 279-290.
43. Wei C., James S., Ye C., Tatam R. and Irving P. (2000) Application issues using fibre Bragg gratings as strain sensors in fibre composites. *Strain* **36**: 143-150.
44. Melle S.M. and Liu K. (1993) Practical fiber-optic Bragg grating strain gauge system. *Appl Optics* **32**: 3601-3609.
45. Rajan G., Ramakrishnan M., Semenova Y., Ambikairajah E., Farrell G. and Peng G.-D. (2014) Experimental study and analysis of a polymer fiber Bragg grating embedded in a composite material. *J Lightwave Technol* **32**: 1726-1733.
46. Du C., Xie W., Meng S., Yin Y., Jiao L. and Song L. (2012) The connection technology based on high temperature silica fiber optic sensor. Proc. SPIE Smart Structures and Materials+ Nondestructive Evaluation and Health Monitoring, 83452X-83452X-83458.
47. Li G.-Y. and Guan B.-O. (2009) The strain response of chemical composition gratings at high temperatures. *Measurement Science and Technology* **20**: 025204.
48. Maier R.R., MacPherson W.N., Barton J.S., Jones J.D., McCulloch S. and Burnell G. (2004) Temperature dependence of the stress response of fibre Bragg gratings. *Measurement Science and Technology* **15**: 1601.
49. Meng S., Du C., Xie W., Huo S., Jiao L., Jin H. and Song L. (2013) Application of high-temperature optical fiber sensor in temperature and strain testing of hot structure. *J Solid Rocket Technol* **36**: 701-705.

50. Du C., Xie W., Huo S., Meng S., Xu K. and Jiao L. (2013) The response of high-temperature optical fiber sensor applied to different materials. Proc. Fourth International Conference on Smart Materials and Nanotechnology in Engineering, 87930O-87930O-87938.
51. Raju S., Sivasubramanian K., Divakar R., Panneerselvam G., Banerjee A., Mohandas E. and Antony M. (2004) Thermal expansion studies on Inconel-600® by high temperature X-ray diffraction. *J Nucl Mater* **325**: 18-25.
52. Corporation S.M. (2008) INCONEL® ALLOY 600. In: Book INCONEL® ALLOY 600, Editor (Ed)^(Eds). Special Metals Corporation, City.
53. HOU X., CHENG W., Ni C. and ZHOU H.-y. (2013) Preparation of a high performance carbon/carbon composite throat insert woven with axial carbon rods. *New Carbon Materials* **28**: 355-362.
54. SHI H.-b., Min T., Bo G. and SU J.-m. (2011) Effect of graphitization parameters on the residual stress in 4D carbon fiber/carbon composites. *New Carbon Materials* **26**: 287-292.
55. Othonos A. (1997) Fiber bragg gratings. *Rev Sci Instrum* **68**: 4309-4341.
56. Barlow A.J. and Payne D.N. (1983) The stress-optic effect in optical fibers. *Quantum Electronics, IEEE Journal of* **19**: 834-839.
57. O'Dwyer M.J., Ye C.-C., James S.W. and Tatam R.P. (2004) Thermal dependence of the strain response of optical fibre Bragg gratings. *Measurement Science and Technology* **15**: 1607.
58. Zaman W., Li K.-z., Li W., Zaman H. and Ali K. (2014) Flexural strength and thermal expansion of 4D carbon/carbon composites after flexural fatigue loading. *New Carbon Materials* **29**: 169-175.
59. Farhan S., Wang R. and Li K. (2015) Directional thermophysical, ablative and compressive behavior of 3D carbon/carbon composites. *Ceram Int* **41**: 9763-9769.
60. YAMAUCHI H., HAYAKAWA H. and SUZUKI S. (2007) Development of three dimensional composite with extremely low thermal expansion properties. *IHI engineering review* **40**: 27-30.